Expanded View Figures

Figure EV1. The CRL4-DCAF1 oligomerization state changes upon neddylation and is dependent on LisH, the DCAF1 dimerization domain.

A Sensitivity score profiles adapted from the DRIVE data for DDB1, DCAF1, DDB2, CRBN, DCAF4, DCAF5, DCAF6, DCAF8, WDTC1, DCAF10, DCAF11, and DCAF12. The dropout score in the shRNA screen was converted into log fold-change (logFC) per shRNA per cell line. The logFC was then normalized per sample to obtain a shRNA level sensitivity score. The shRNA level scores are further aggregated to gene level sensitivity scores using either the ATARiS algorithm (Shao *et al*, 2013) or the RSA algorithm (König *et al*, 2007). These give a measure of the statistical significance of the dropout of those 20 shRNAs used per gene compared to the remainder shRNAs in the screen (McDonald *et al*, 2017).

B Domain organization of human CUL4A, DDB1, and RBX1. CR, cullin repeat; UFD, ubiquitin-fold domain; RING, really interesting new gene; WH, winged helix; BP, β-propeller.

C SEC-MALS analysis, the chromatogram shows the Rayleigh ratio curves of $CRL4^{DCAF1}$ (FL), $CRL4^{DCAF1(\Delta NTD)}$, and DDB1-DCAF1 (FL) together with the molar mass (MDa) of the main peaks determined by MALS. The table summarizes the SEC-MALS observed molecular weights, the calculated molecular weight, polydispersity values, and oligomeric states of the tested complexes.

D SDS–PAGE of the corresponding complexes.

Source data are available online for this figure.

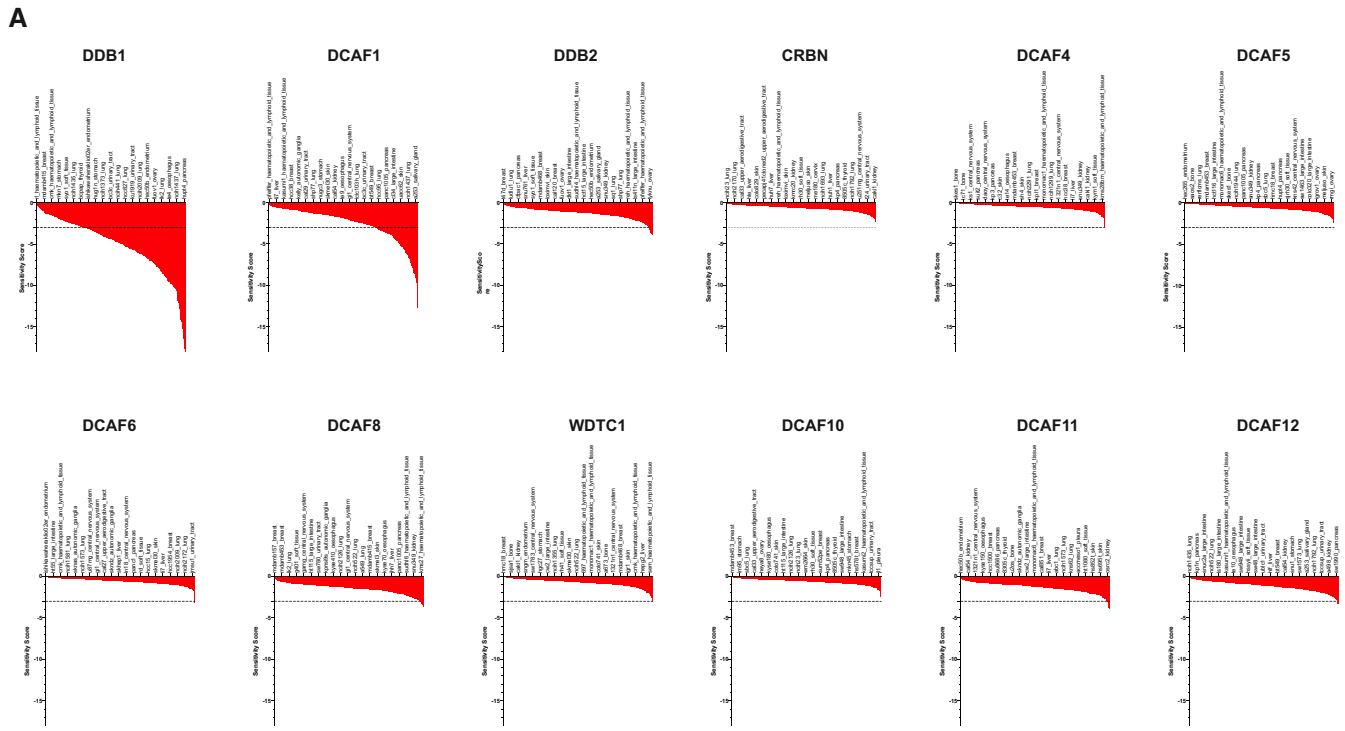

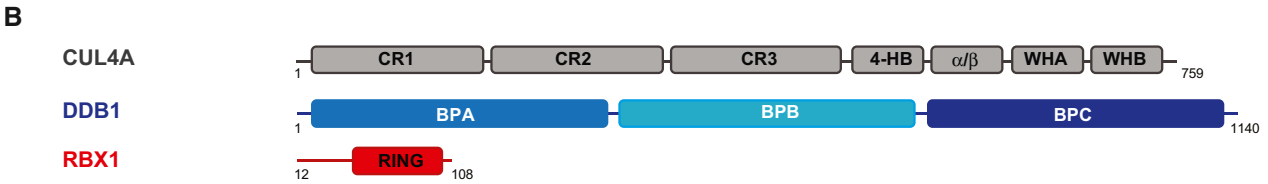

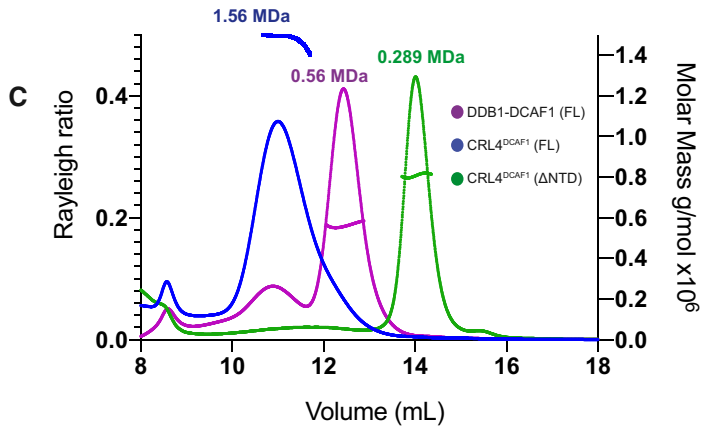

Sample	Observed Mwt g/mol	Expected Mwt g/mol	Poly-dispersity (Mw/Mn)	Oligomeric 1state
DDB1-DCAF1 (FL)	0.563×10^6	0.592×10^6	1.000	Dimer
$CRL4^{DCAF1}$ (ΔNTD)	0.289×10^6	0.287×10^6	1.002	Monomer

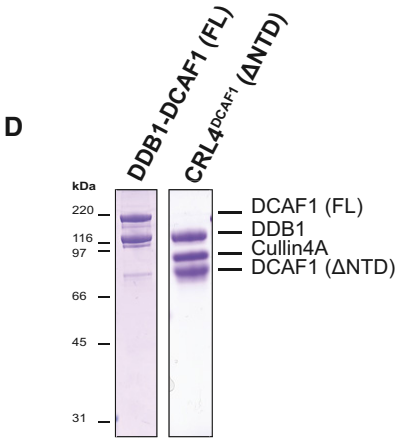

Figure EV1.

Figure EV2. Cryo-EM data analysis, classification, and refinement procedures for the CRL4^{DCAF1} complex.

A Representative micrograph for CRL4^{DCAF1} complex.

B Workflow of cryo-EM classification and refinement.

C Fourier shell correlation curve (FSC). The resolution values reported for all reconstructions are based on the gold-standard Fourier shell correlation curve (FSC) at 0.143 criterion and all the related FSC curves are corrected for the effects of soft masks using high-resolution noise substitution.

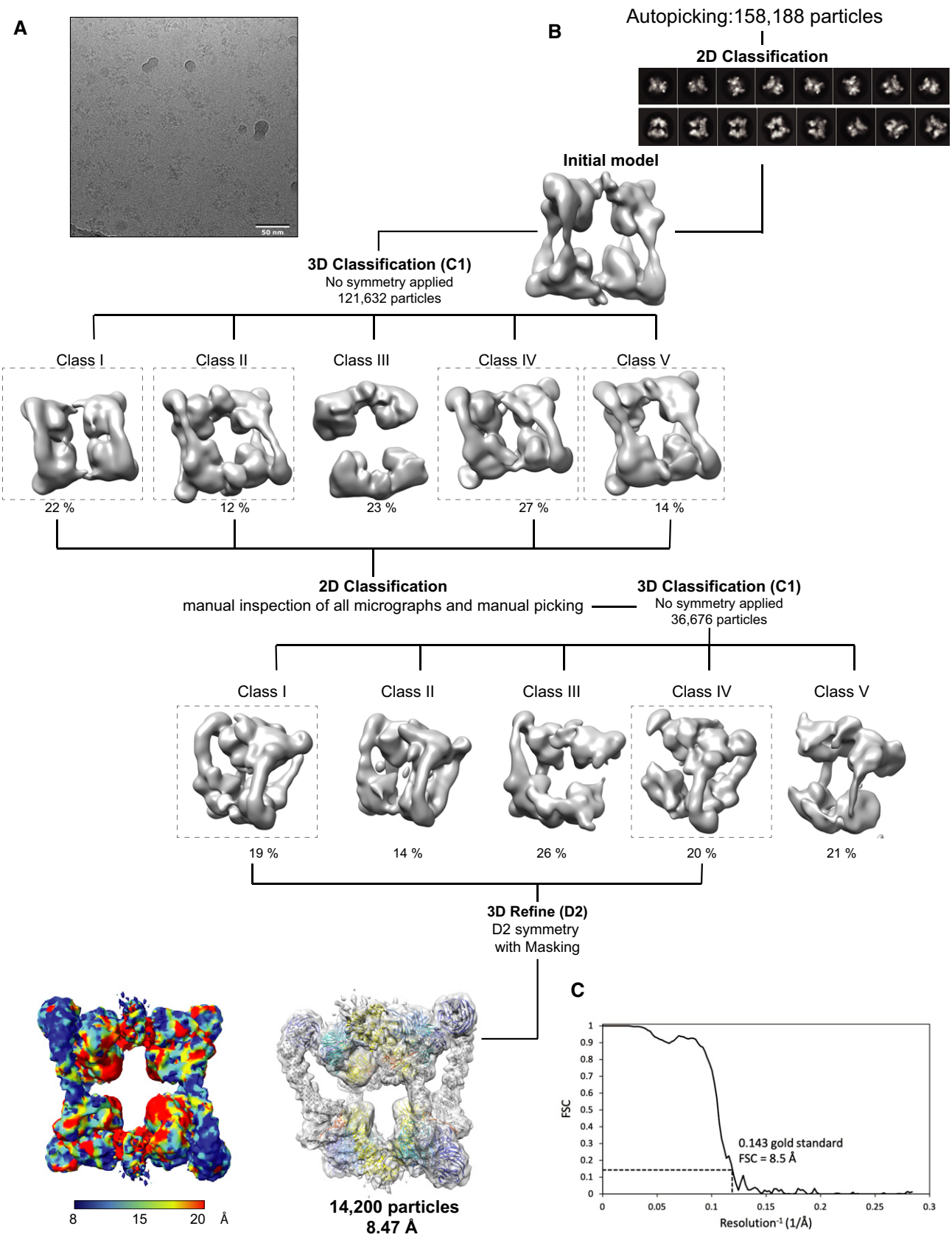

Figure EV2.

Figure EV3. Modeling the ARM and LisH domains of DCAF1 N-terminus into the CRL4^{DCAF1} cryo-EM map.

A Different rotation views of DCAF1 ARM domain (brown) and LisH domain (light orange) modeled into the CRL4^{DCAF1} cryo-EM map. Three potential docking poses of the ARM domain are shown in the upper, middle, and lower panels. The correlations between simulated 8.4 Å model maps and the experimental map are 0.53, 0.59, and 0.59 (from top to bottom). LisH helices are labeled as $H2^1$, $H3^1$ from one molecule and $H2^2$, $H3^2$ from the other protomer. The resolved part of the ARM repeats spanning residues (507–817) and excluding insertions are labeled as ARM (1 to 5). The unmodeled linker between DCAF1-ARM and LisH domains is indicated by a red dashed line. The map contour level is 0.00934.

B Symmetric docking of LisH homodimer. The root mean square (r.m.s.) deviation was calculated by comparing the decoys against the modeled homodimer based on the LisH domain extracted from coordinates with PDB ID 6IWV.

C Fitting of the LisH domain. The map contour level is 0.0132.

D Initial ARM domain model from the *Alphafold* pipeline. The part fitted into the density is colored in orange (left). In the right panel, the ARM domain is colored according to pLDDT values (predicted local distance difference test; scale 0–100, low to high confidence, Jumper *et al*, 2021).

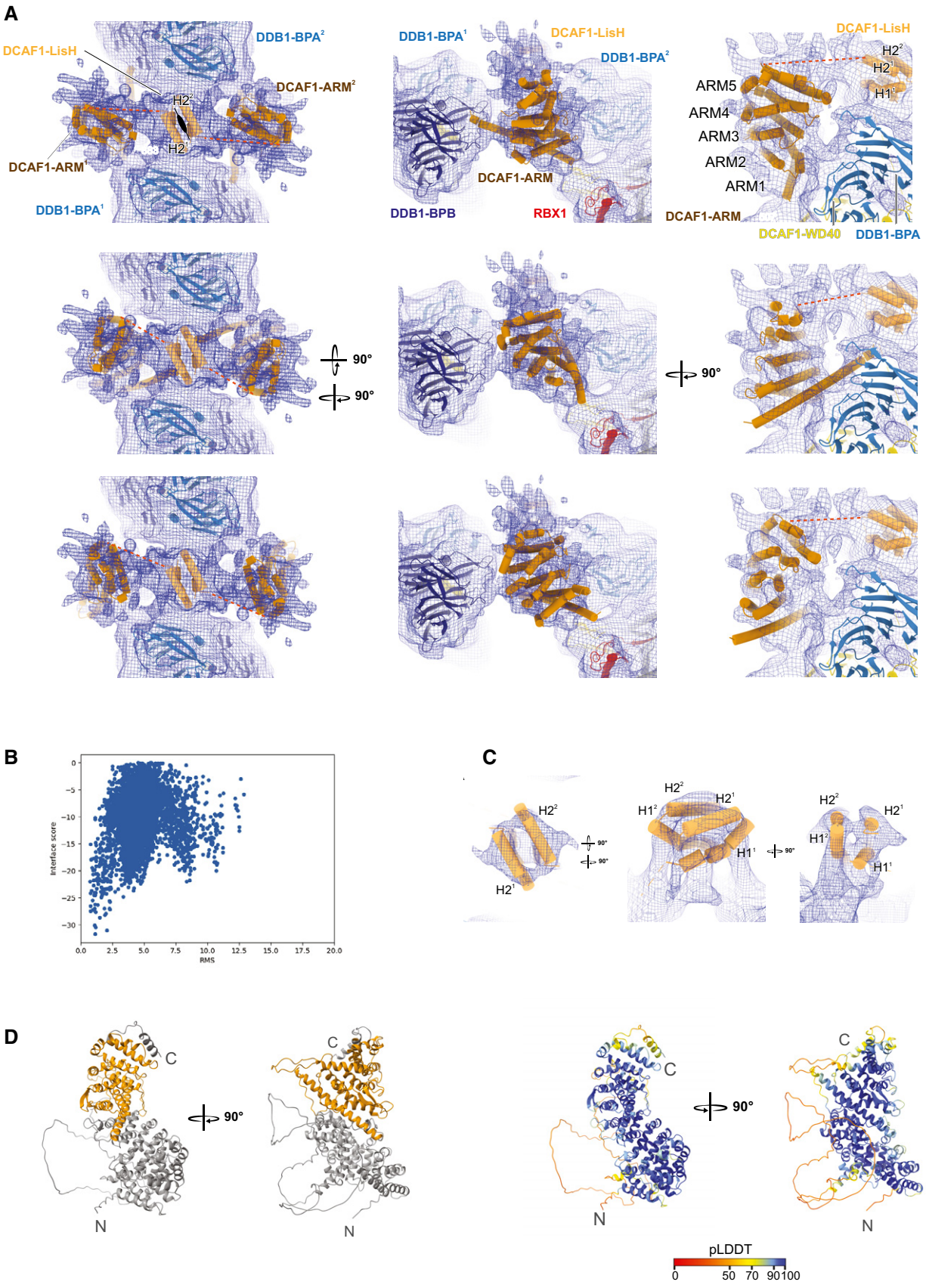

Figure EV3.

Figure EV4. CRL4^{DCAF1} tetramerization and CSN binding are mutually exclusive.

A Fitting the crystal structure of CSN (PDB 4D10) (wheat) into CRL4^{DCAF1} cryo-EM map.

B Strep pull-down assay of untagged CSN (E76A) complex on strep-tagged N8-CRL4^{DCAF1}(FL) (lane1), CRL4^{DCAF1}(FL) (lane2), CRL4$^{DCAF1(\Delta NTD)}$ (lane3), and N8-CRL4$^{DCAF1(\Delta NTD)}$ (lane 4) (n = 2).

C A representative cryo-EM micrograph for CRL4^{DCAF1}-CSN complex.

D Workflow of cryo-EM classification and refinement.

E Fourier shell correlation curve (FSC). The resolution values reported for all reconstructions are based on the gold-standard Fourier shell correlation curve (FSC) at 0.143 criterion and all the related FSC curves are corrected for the effects of soft masks using high-resolution noise substitution.

Source data are available online for this figure.

© 2021 The Authors

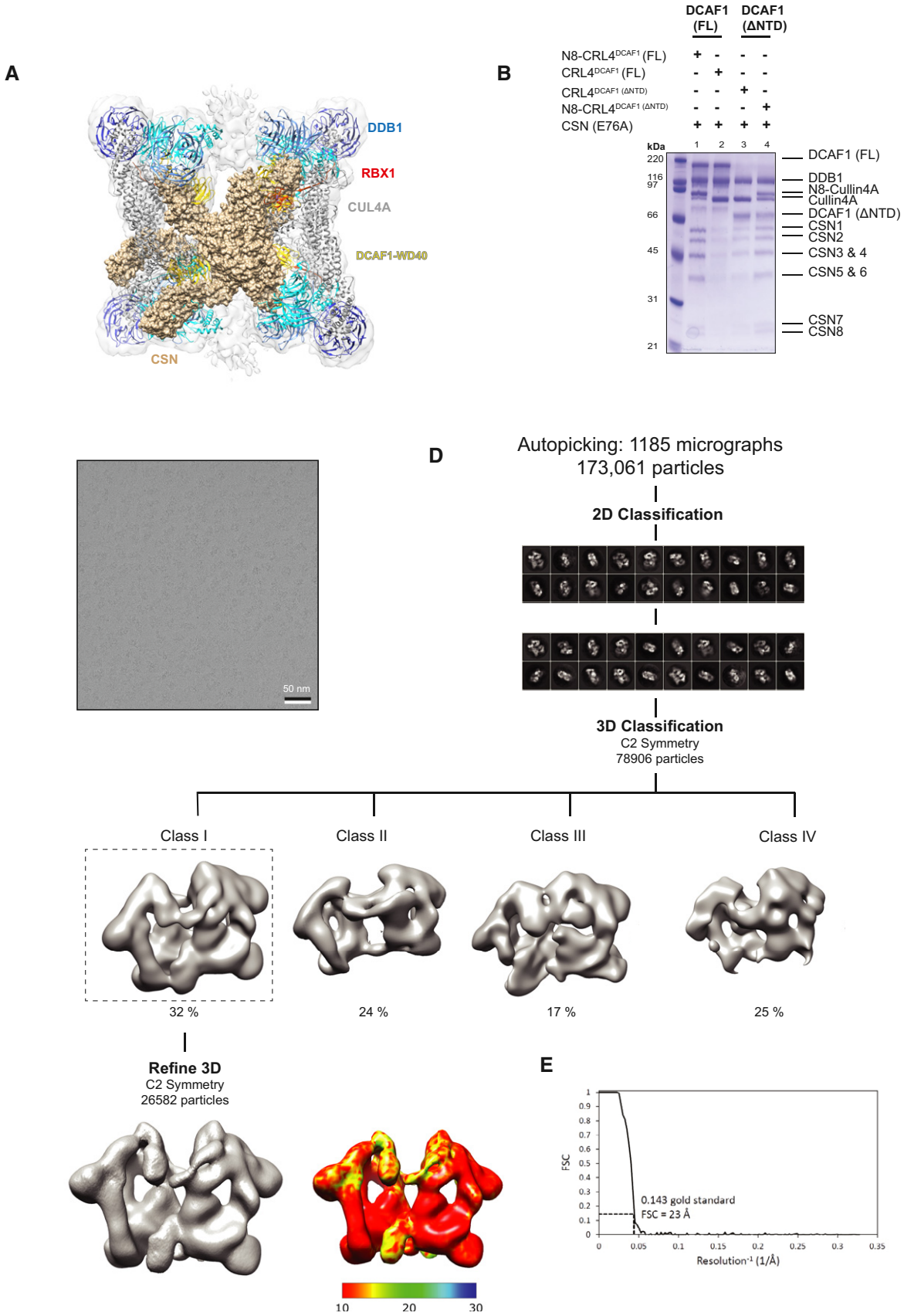

Figure EV4.

Figure EV5. CSN catalysis on UNG2- and MERLIN-bound N8-CRL4^{DCAF1}.

A–C SEC-MALS analysis including the peaks eluting near the SEC column void volume of (A) CRL4^{DCAF1}-VPR, (B) CRL4^{DCAF1}-VPR-UNG2, and (C) CRL4^{DCAF1}-MERLIN. The chromatogram shows the Rayleigh ratio curves together with the molar mass (MDa) determined by MALS.

D A close-up view of The CRL4^{DCAF1}-CSN cryo-EM map with fitted crystal structures of CUL4A (gray), RBX1 (red) (PDB 2HYE), DDB1 (blue)-DCAF1 (WD40) (yellow), VPR (dark gray), and UNG2 (green) (PDB 5JK7).

E, F Fluorescence polarization assay investigating the catalytic activity of CSN on N8-CRL4^{DCAF1}(FL) when bound to (E) VPR-UNG2 or (F) MERLIN. Initial rates (M/s) are plotted versus concentrations (M) of N8-CRL4^{DCAF1}(FL)-VPR-UNG2 (magenta), N8-CRL4^{DCAF1}(FL) (blue), and N8-CRL4^{DCAF1}(FL)-MERLIN (red). Column representation of K_{cat} values, and table summarizes K_M, K_{cat}, and V_{max} values calculated from the curves (biological replicates, $n = 3$, mean ± SD).

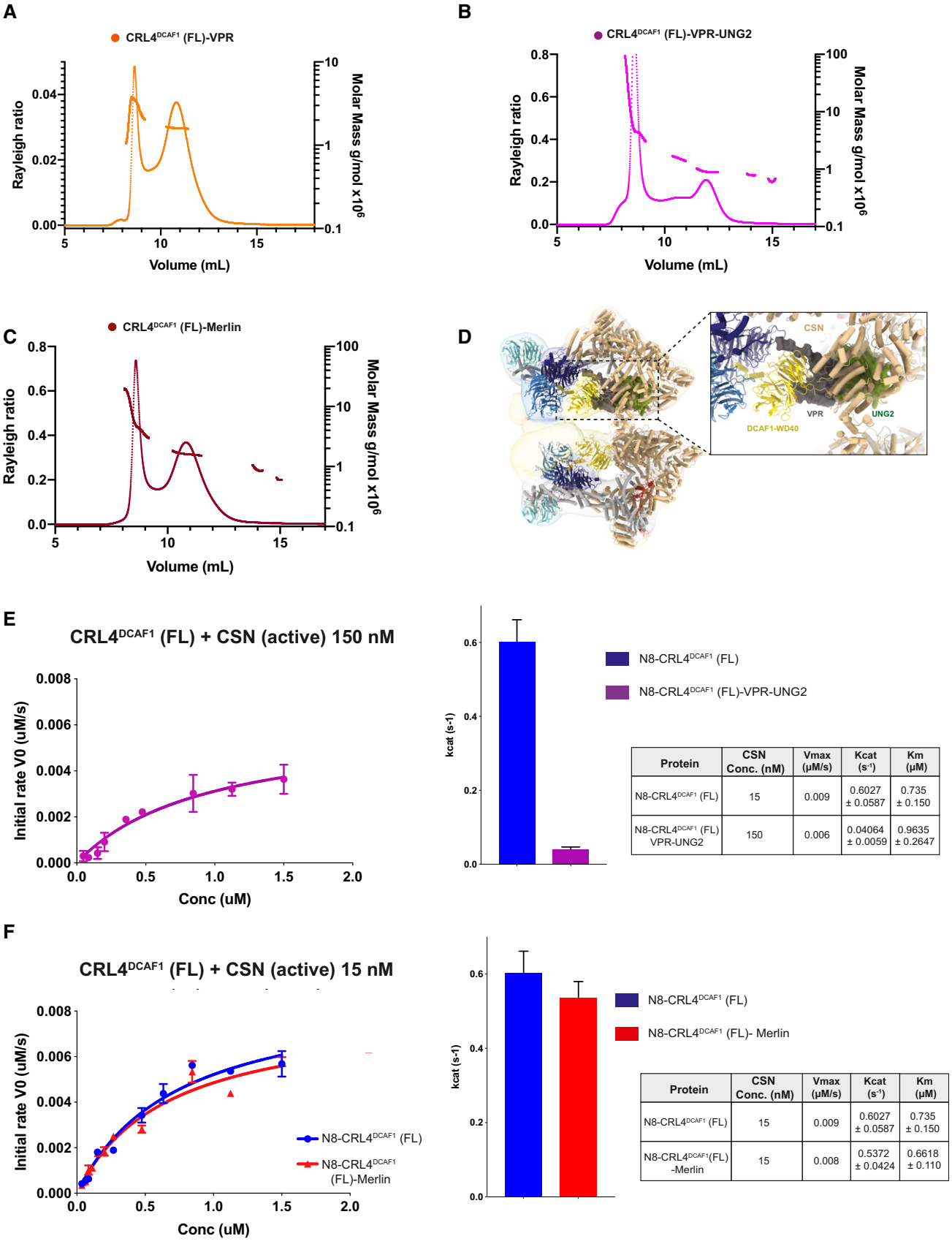

Protein	CSN Conc. (nM)	Vmax (μM/s)	Kcat (s^{-1})	Km (μM)
N8-CRL4^{DCAF1} (FL)	15	0.009	0.6027 ± 0.0587	0.735 ± 0.150
N8-CRL4^{DCAF1} (FL) VPR-UNG2	150	0.006	0.04064 ± 0.0059	0.9635 ± 0.2647

Protein	CSN Conc. (nM)	Vmax (μM/s)	Kcat (s^{-1})	Km (μM)
N8-CRL4^{DCAF1} (FL)	15	0.009	0.6027 ± 0.0587	0.735 ± 0.150
N8-CRL4^{DCAF1}(FL) -Merlin	15	0.008	0.5372 ± 0.0424	0.6618 ± 0.110

Figure EV5.